J|A|C|S
ARTICLES
Published on Web 03/02/2006

Microfaceting Explains Complicated Structures on Rutile TiO_2 Surfaces

Toshitaka Kubo,* Kazuhiro Sayama, and Hisakazu Nozoye†

Contribution from the National Institute of Advanced Industrial Science and Technology (AIST), Tsukuba Central 5-2, 1-1-1 Higashi, Tsukuba, Ibaraki 305-8565, Japan

Received November 20, 2005; E-mail: t-kubo@aist.go.jp

Abstract: Surface structures on rutile TiO_2 (001) have been studied by using scanning tunneling microscopy (STM), X-ray photoelectron spectroscopy (XPS), and density functional calculations. Prior investigations have observed many kinds of complicated surface structures; however, detailed atomic structures and the mechanism of the reconstructions are still unknown. We evaluate the energetical stability of the surface structures. The calculational results suggest that a {111} microfaceting model is energetically stable compared with the unreconstructed (1 × 1) model. We propose microfaceting structural models that are in good agreement with atomically resolved STM images. This structural concept can be extended to other rutile TiO_2 surfaces in general.

I. Introduction

It has been well-known that the chemical reactivity of catalytic materials strongly depends on the very tiny differences in preparation methods and conditions. Structure determination of reactive metal oxide surfaces is very important in understanding the catalytic process in which chemical reactions occur. However, surfaces of many metal oxide materials exhibit quite complicated and long-range structures;[1,2] little is known about the general view of reconstructions, even on the most extensively investigated Titania (titanium dioxide: TiO_2) surfaces. Among metal oxide materials, TiO_2 has been attracting extensive attention because of its great importance in several technological applications including catalysis, photocatalysis, super-hydrophilicity, sensors, and so on.[2−4] In this study, atomic structures and mechanisms of the surface reconstructions on rutile TiO_2 (001), which is the least stable among the low-index surfaces, have been studied by using scanning tunneling microscopy (STM), X-ray photoelectron spectroscopy (XPS), and density functional calculations. We propose microfaceting structural models that are in good agreement with atomically resolved STM images. In addition, the driving force of the microfaceting reconstructions is discussed.

II. Experimental Section: Materials and Setup

Two types of ultrahigh vacuum apparatus have been used: one for STM (JEOL: JSTM-4610) with a base pressure of 1.2×10^{-8} Pa and the other for XPS (ULVAC−PHI: XPS-1800) with a base pressure of 2.4×10^{-8} Pa. STM measurements were performed at room temperature in a constant-current condition. Tips used for STM measurements were prepared by electrochemical etching of a tungsten wire in NaOH solution. XPS spectra were recorded using a 400 W Al Kα radiation.

A TiO_2 (001) substrate of $7 \times 1 \times 0.5$ mm^3 (Nakazumi Crystal) was directly mounted on a silicon heater. The sample surface was cleaned by several cycles of Ar^+-ion sputtering (2 keV) and annealing. The surface cleanliness was checked by XPS. Vacuum pressure during annealing did not exceed 5×10^{-7} Pa. The typical heating rate and cooling rate were several °C/s. Temperature was measured with an optical pyrometer.

III. Theoretical Section: Calculation Details

Density functional calculations were performed at Tsukuba Advanced Computing Center (TACC) by an ultrasoft pseudopotential technique with a plane-wave basis. In this method, valence electron wave functions were obtained by minimizing the Kohn−Sham total-energy function.[5] The exchange correlation potential was treated with the generalized gradient approximation (GGA).[6] The self-consistent ultrasoft pseudopotential proposed by Vanderbilt was used for electron−ion interaction.[7] The criteria of energy change per atom, root-mean-square (RMS) displacement of atoms, and RMS force on each atom were 2.0×10^{-5} eV/atom, 0.01 Å, and 0.05 eV/Å, respectively. Gaussian smearing of 0.2 eV was used.

The unreconstructed and the {111} microfaceting surfaces of TiO_2 (001) were modeled by periodic slabs. The periodic slabs consisted of 10 atomic layers, which were isolated by $3 \times a_{TiO2}$ width of vacuum regions. Atoms at the central two layers were fixed at the bulk position; all other atoms were geometry optimized.

IV. Results and Discussion

To elucidate the atomic structures of the reconstructions, several surface structures on TiO_2 (001), which were prepared by systematically changing sample preparation conditions, were examined in an atomic scale by STM. Figure 1a shows an STM

† Current address: ULVAC−PHI Inc., 370 Enzo, Chigasaki, Kanagawa, 253-0084, Japan.

(1) Lüth, H. *Surfaces and Interfaces of Solid Materials*; Springer: New York, 1995.
(2) Henrich, V. E.; Cox, P. A. *The Surface Science of Metal Oxides*; Cambridge University Press: Cambridge, 1994.
(3) Bonnell, D. A. *Prog. Surf. Sci.* **1998**, *57*, 187.
(4) Diebold, U. *Surf. Sci. Rep.* **2003**, *48*, 53.
(5) Kohn, W.; Sham, L. J. *Phys. Rev.* **1965**, *140*, A1133.
(6) Perdew, J. P. *Physica B* **1991**, *172*, 1.
(7) Vanderbilt, D. *Phys. Rev. B* **1990**, *41*, 7892.

10.1021/ja0578808 CCC: $33.50

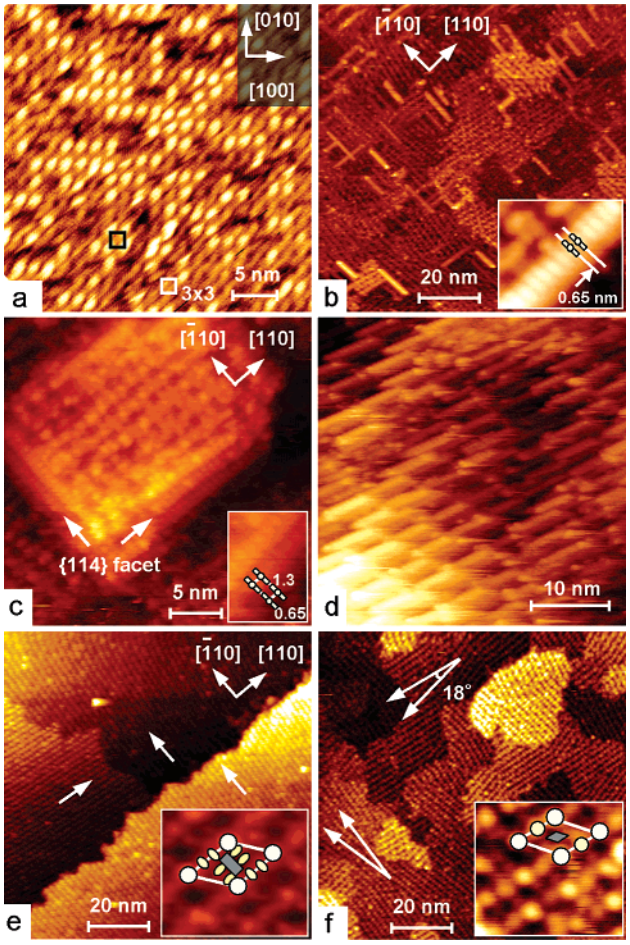

Figure 1. STM images of the TiO_2 (001) surface reconstructions. (a) Mixture of missing and added (3 × 3) dot structures (35 × 35 nm^2, 0.04 nA, 2.5 V), (b) isolated row structure (100 × 100 nm^2, 0.06 nA, 2.6 V; (inset) 6.6 × 5.7 nm^2, 0.03 nA, 2.5 V), (c) {114} faceted row structure (30 × 30 nm^2, 0.02 nA, 1.75V; (inset) 7.6 × 11 nm^2, 0.02 nA, 1.75V), (d) ordered {114} faceted row structure (40 × 40 nm^2, 0.02 nA, 2.5V), (e) ridge-like $\begin{pmatrix} 5 & 2 \\ 4 & 4 \end{pmatrix}$ structure (100 × 100 nm^2, 0.02 nA, 2.5 V; (inset) 10.6 × 9.2 nm^2, 0.02 nA, 3.2 V), and (f) ridge-like $\begin{pmatrix} 5 & \bar{1} \\ 4 & 3 \end{pmatrix}$ structure (100 × 100 nm^2, 0.05 nA, 3.0 V; (inset) 7.4 × 6.7 nm^2, 0.06 nA, 3.0 V). Arrows indicate the directions of main ridges.

image of dot-like structures. The structure was obtained after the sample was annealed in the air at 600 °C for 3 h and annealed in UHV at 1000 °C for 30 min. Bright and dark dots arranged in intervals of 1.4 nm along [100] and [010], which form small 3 × 3 domains, were observed. Figure 1b shows an isolated row structure, which runs along [110] or [$\bar{1}$10] directions formed on the defective terraces. The structure was obtained after the sample was sputtered, subsequently flashed to 800 °C, and then quenched. In an atomically resolved STM, which is shown in the inset of Figure 1b, narrow-rectangular spots, which are lined perpendicular to the row, are arranged with a distance of 0.65 nm along the row, the center of which is slightly brighter than both sides. The observed row structure is considered to be the same as in previously reported results.[12−14] At the edges of a hill-like structure on the same sample, an arranged row structure, which was located on a {114} slope, was observed, as shown in Figure 1c. The atomic structure of each row seems to be the same as that of the isolated row structure, as shown in the inset of Figure 1c. With further annealing at 1200 °C for 30 min, an ordered {114} faceted row structure was observed, as shown in Figure 1d. Figure 1e shows a ridge-like structure with main ridges separated by 2.3 nm. The structure was obtained after the sample was sputtered and subsequently annealed at 600 °C for several seconds. The directions of the main ridges, which run along [110] and [$\bar{1}$10], alternatively rotate by 90° between consecutive terraces. In a magnified image, which is shown in the inset of Figure 1e, ridges of lesser height running perpendicular to the main ridges are observed. Bright spots and a dark depression are additionally observed at the corner and the mid positions of a unit cell lattice, respectively. Figure 1f shows another kind of ridge-like structure. The structure was obtained after the sample was further annealed at 800 °C for several seconds. Main ridges show two domains on the same terrace. The directions of the ridge in the same terrace are different by 18°, thus forming four domains in the whole surface. In a magnified image, there are two kinds of bright spots in the unit cell lattice, as shown in the inset of Figure 1f. The brightest spots, the next brightest spots, and the dark depression are observed at the cell corner, middle of the brightest spot along the main ridge, and the mid positions of unit cell lattice, respectively. Although both the ridge-like structures contain many kinds of defects and dislocations, the structures have more than several atomic layers height, and typical surface unit cell lattices are $\begin{pmatrix} 5 & \bar{2} \\ 4 & 4 \end{pmatrix}$ and $\begin{pmatrix} 5 & \bar{1} \\ 4 & 3 \end{pmatrix}$, respectively. We observed many kinds of surface structures including defective structures and the structure, that did not have surface 2D symmetry. However, the unreconstructed TiO_2 (001)−(1 × 1) structure was not observed in our experimental conditions.

When a metal oxide sample is annealed in an ultrahigh vacuum, the sample is generally reduced; i.e., oxygen vacancy defects are formed.[1−4] It is well-known that many metal oxide materials exhibit various kinds of nonstoichiometric suboxide surface structures. To clarify whether the observed reconstructions are related to the nonstoichiometric suboxide structures or not, the concentration of the oxygen vacancy in TiO_2 (001) by heating was examined by XPS, as shown in Figure 2. Figure 2a shows Ti 2p XPS spectra of TiO_2 (001) after annealing at 500 °C for 60 min. The formal ionic charge of Ti in the stoichiometric TiO_2 crystal is Ti^{4+}. The peaks of Ti^{4+} ($2p_{1/2}$) and Ti^{4+} ($2p_{3/2}$) were observed at 465.0 and 459.3 eV, respectively. Figure 2b shows Ti 2p XPS spectra of TiO_2 (001) after annealing at 1200 °C for 5 min. When oxygen vacancy defects are created, nearest Ti atoms form a lower oxidation state as Ti^{3+}, which can be seen by the small shoulder to the right of the main Ti^{4+} (2p) peak. The signal intensity of the Ti^{3+} peaks depends on the concentration of the oxygen vacancy. To estimate the concentration of the oxygen vacancy by heating, changes of the Ti^{3+} 2p XPS spectra of TiO_2 (001) by heating were shown in Figure 2c−g. When the sample was annealed higher than 1000 °C, Ti^{3+} 2p XPS peaks appeared 1.7 eV lower than Ti^{4+} peaks. The peak is increased with increasing annealing temperature, suggesting that the oxygen vacancy defects are increased. We estimated the concentration of the oxygen

(8) Kasowski, R. V.; Tait, R. H. *Phys. Rev. B* **1979**, *20*, 5168.
(9) Ramamoorthy, M.; Vanderbilt, D.; King-Smith, R. D. *Phys. Rev. B* **1994**, *49*, 16721.
(10) Firment, L. E. *Surf. Sci.* **1982**, *116*, 205.
(11) Poirier, G. E.; Hance, B. K.; White, J. M. *J. Vac. Sci. Technol. B* **1992**, *10*, 6.
(12) Nörenberg, H.; Dinelli, F.; Briggs, G. A. D. *Surf. Sci.* **1999**, *436*, L635.
(13) Fukui, K.; Tero, R.; Iwasawa, Y. *Jpn. J. Appl. Phys.* **2001**, *40*, 4331.
(14) Tero, R.; Fukui, K.; Iwasawa, Y. *J. Phys. Chem. B* **2003**, *107*, 3207.

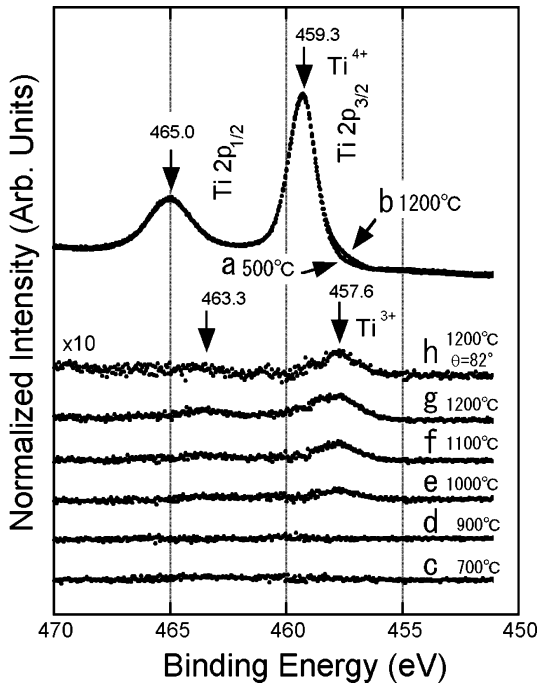

Figure 2. Ti 2p XPS spectra of TiO_2 (001) after annealing at (a) 500 °C for 60 min and (b) 1200 °C for 5 min. Difference spectra of TiO_2 (001) after annealing at (c) 700 °C for 60 min, (d) 900 °C for 60 min, (e) 1000 °C for 60 min, (f) 1100 °C for 10 min, (g) 1200 °C for 5 min (Figure 2b), and (h) 1200 °C for 5 min compared to the TiO_2 (001) after annealing at 500 °C for 60 min (Figure 2a). Electron emission angle shown in Figure 2a−g and 2h were 0° and 82° with respect to the surface normal, respectively.

vacancy by the signal intensity ratios (Ti^{3+}/Ti^{4+}) of the Ti ($2p_{3/2}$) line. The ratios were under detection limit (annealing at ≤ 900 °C), 0.9% (1000 °C), 1.5% (1100 °C), and 1.9% (1200 °C). The concentration of the oxygen vacancy seems to be negligible; however, it is known that the typical information depth of the XPS is on the order of several nm,[1] which corresponds to more than 10 atomic layers of the TiO_2 (001) surface. To clarify whether the Ti^{3+} 2p XPS signals come from the top surface or the bulk regions, we also measured the angle-dependent Ti 2p XPS spectra on the slightly reduced TiO_2 (001) at the electron emission angle between 0 and 82° with respect to the surface normal. Difference spectra compared to the TiO_2 (001) after annealing at 500 °C for 60 min (Figure 2a) were shown in Figure 2, g (detector: surface normal) and h (detector: 82° with respect to the surface normal). The information depth of the XPS measurement at electron emission angle of 82° corresponds to several atomic layers depth. The results show that angle-dependent changes of the peak intensity ratio were not observed, suggesting that the concentration of the oxygen vacancy at the surface layers are almost the same as the bulk region. It is concluded that the oxygen vacancy does not concentrate at the surface region even on slightly reduced TiO_2 (001). Most of the present and previously observed structures[12−14] have more than several atomic layers height. Supposing that these structures are mainly based on the nonstoichiometric suboxide structures, such as Ti_2O_3, Ti_3O_5, and so on, the structures contain a considerable amount of Ti^{3+} atoms. These Ti^{3+} XPS peaks must be detectable in the angle-dependent XPS measurement. Furthermore, many of the observed surface structures, such as the row structures and the ridge-like structures, were formed at a temperature of 600−800 °C. In this temperature range, the concentration of the oxygen vacancy is lower than the detection limit in our XPS measurements. Although a small amount of the nonstoichiometric suboxide structures may locally exist on the surface, these must be very minor species. We conclude that the nonstoichiometric suboxide surface structural models cannot explain observed surface structures in general.

Next, energetical stability of reconstructed (001) surface is discussed by calculations. The crystal structure of rutile-type TiO_2 is tetragonal and contains six atoms in a unit cell. Each Ti atom is coordinated to six neighboring O atoms, and each O atom is coordinated to three neighboring Ti atoms. The most stable surface among the low-index surfaces is (110), which has the least density of dangling bond (DB: unsaturated coordination) with 5-fold or 6-fold coordinated surface Ti atoms. On the other hand, for the unreconstructed (001) surface, which is nonpolar but the least stable of the low-index surfaces, all of the surface Ti atoms are 4-fold coordinated. The surface energy of the (001) surface was calculated to be 23.4 meV/au^2, which is almost twice the value of the (110) surface (12.1 meV/au^2). Previous calculations have shown that the (001) surface is thermodynamically unstable.[8,9] It is believed that the high surface energy associated with this high degree of coordinative unsaturation is one of the driving forces for faceting, roughening, and reconstruction.[8−14] Two 5-fold coordinated Ti atoms can replace a 4-fold coordinated Ti atom by a simple operation with the surface stoichiometry unchanged, e.g., formation of a missing or an added TiO_2 defect (Figure 3a). To improve calculational accuracy, a missing and added TiO_2 defect pair (2×2) model was used in this study. When a TiO_2 unit is removed (or added) on the surface, a 4-fold coordinated Ti atom (which has two DBs) disappears and two 5-fold coordinated Ti atoms (which has one DB) appear. For both of the operations, the total number of DBs is unchanged. However, surface energy of the defect model is calculated to be stable by 1.97 meV/au^2 (8.4%) compared with that of the unreconstructed TiO_2 (001) model. Supposing that the surface energies for missing and added TiO_2 structures are almost the same, the surface is stabilized about 0.6 eV by a single TiO_2 defect formation. This may be the driving force of the reconstructions and induce the complicated surface structures, as shown in Figure 3b−d.

For the semiconductor and the ionic materials, surface energy is mainly stabilized by saturation of free DBs, decrease of the Madelung (electrostatic) interaction, and so on.[1] In the present case, the unreconstructed surface is originally nonpolar and the number of the DBs could not be decreased by the TiO_2 defect formations. A more detailed discussion has to be considered. Atomic relaxations of each model are summarized in Table 1. For the unreconstructed model, we can see large rumpling and lattice distortion at the surface region, which extend to deeper layers. The changes of the interlayer spacing and the standard deviations of vertical atomic coordinates at the surface region are calculated to be larger than 10% and 0.2, respectively. On the other hand, the lattice distortions of the missing or added models are relatively small. The changes of the overall electron orbital energy due to the lattice relaxation are considered to stabilize the surface energy and induce the defect formations.

Next, we mention the physical meaning of the defect formations (replacement of a 4-fold coordinated Ti atom by two 5-fold coordinated ones). As the direction of a Ti−O bond in a bulk crystal is aligned along [110] or [111], the 5-fold

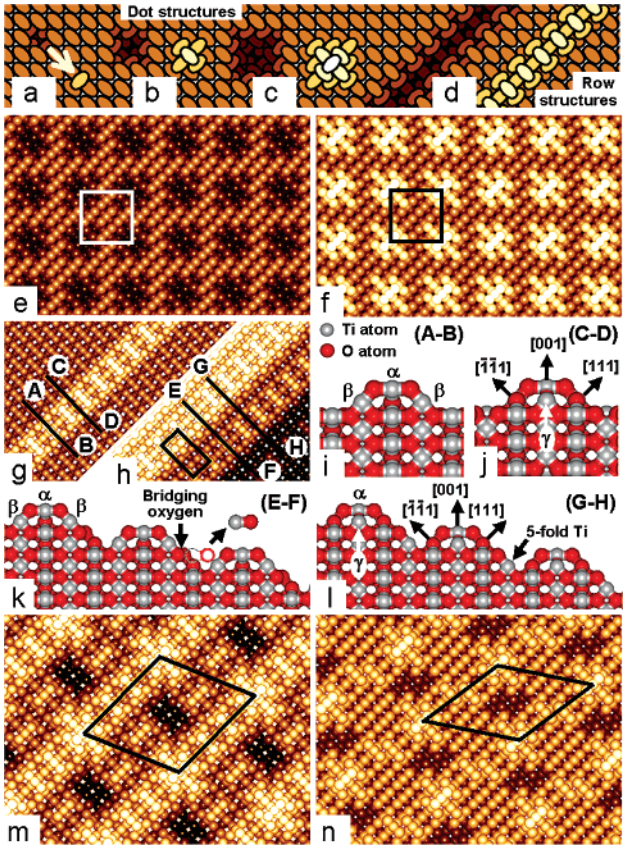

Figure 3. Schematic illustration of missing and added TiO_2: (a) single units, (b) pentamers, (c) 14-mers, and (d) row structures. An oval shows a TiO_2 unit. Proposed structural models of TiO_2 (001): (e) missing dot-like (3 × 3) structure, (f) added dot-like (3 × 3) structure, (g) isolated row structure, and (h) {114} faceted row structure. (i and j) Cross-sectional views of isolated row structure along the lines (A−B) and (C−D), respectively. (k and l) Cross-sectional views of {114} faceted row structure along the lines (E−F) and (G−H), respectively. Typical structural models of TiO_2 (001) ridge-like (m) $\begin{pmatrix} 5 & 2 \\ 4 & 4 \end{pmatrix}$ and (n) $\begin{pmatrix} 5 & 1 \\ 4 & 3 \end{pmatrix}$ structures.

Table 1. Standard Deviations (σ) of Vertical Atomic Coordinates for Each Layer and Relative Interlayer Spacings ($d_{l,l+1}/d_0$) with Respect to Bulk Value

layer	unreconstructed (1 × 1)	added	missing
σ_{added}		0.158	
σ_1	0.200	0.155	0.174
σ_2	0.203	0.183	0.164
σ_3	0.088	0.045	0.117
σ_4	0.062	0.056	0.057
$d_{added,1}/d_0$		−3.04%	
$d_{1,2}/d_0$	−11.49%	−3.31%	−7.59%
$d_{2,3}/d_0$	12.44%	7.10%	6.30%
$d_{3,4}/d_0$	−5.88%	−3.11%	−2.23%
$d_{4,5}/d_0$	3.31%	−0.74%	0.18%

coordinated surface Ti atoms form a {110} or {111} microfacet. The {110} facet is perpendicular to the (001) surface; formation of the {110} facets only increases additional surface area. The (001) surface cannot be stabilized by the formation of {110} facets. Thus, the corresponding operation is equivalent to the formation of stable {111} microfacets in this case. It is worth noting that all of the observed {111} facets are very small in size. Macroscopic {111} facets are not reported on TiO_2 (001).[11−14] These may suggest that macroscopic {111} facets do not stabilize the surface energy, compared with the formation of the {111} microfacets. The bulk-terminated (111) surface is composed of TiO_4 and Ti alternative layers. As the formal ionic charge of Ti and O in the stoichiometric TiO_2 crystal are Ti^{4+} and O^{2-}, respectively, both the terminated layers are polar plane. To reduce Madelung (electrostatic) potential, it is considered that macroscopic {111} facets were not formed on the (001) surface.

We propose {111} microfaceting surface structural models, as shown in Figure 3e−n. The models for the dot-like structures (Figure 1a) can be explained by the missing or added TiO_2 pentamer (Figure 3b) arranged with 3 × 3 periodicity, as shown in Figure 3e and f. For the isolated row structure (Figure 1b), four TiO_2 units are added per unit cell (Figure 3d), and 4-fold coordinated Ti atoms on the (001) terrace are partially replaced by the 5-fold coordinated Ti atoms, as shown in Figure 3g, i, and j. Our calculations show that the observed STM spots are related to a 4-fold coordinated Ti atom located at a center of the row and two 5-fold Ti atoms located at side positions of the row (discussed below), which are tentatively denoted by α- and β-Ti, respectively. For the {114} faceted row structure (Figure 1c and d), the ratio of the 5-fold β-Ti is larger than the isolated row structure, and on top of each terraces, the atomic structure is the same of the isolated row structure (Figure 3h, k, and l). In this case, to form a (111) microfacet plane, a TiO unit is removed (Figure 3k and l). At the same time, one 4-fold α-Ti is replaced by one 5-fold β-Ti, resulting in the formation of bridging oxygen. The decrease of the unsaturated coordination is related to the stabilization of the surface energy. The models for the ridge-like structures (Figure 1e and f) are shown in Figure 3m and n, respectively. Although observed structures contain many kinds of defects and dislocations, all of the STM images can be explained by the {111} microfaceting models. In addition, observed defects and dislocations can be explained by combinations of the missing and (or) added TiO_2 defect formation.

For the early works of the rutile TiO_2 (001) surface, many kinds of faceted structures have been reported, e.g., {011}, {114}, and other minor faces.[10,11] These faceted structures are also explained by our structural models; i.e., the {114} faceted structure consists of the (001), (111); and ($\bar{1}\bar{1}$1) microfacets (Figure 3h, k, and l) and the {011} faceted surface consists of the (111) and ($\bar{1}$11) microfacets, etc. Nörenberg et al. reported several kinds of network structures whose unit-cell vectors were different from our results.[12] However, local structures are quite similar to our results and are considered to be composed of the combinations of {111} microfacets. Recently, Tero et al. proposed a nonstoichiometric added-row model for the {114} faceted row structure.[14] We examined their model by the calculational methods. However, the results show that the model has a huge stress due to the interstitial Ti atoms in the surface region and outermost oxygen atoms being pushed into vacuum (not shown). Calculational results suggest that their structural model is unstable. Instead of their model, to analyze the STM image (Figure 4a), the orbital density and its shapes of the states near the bottom of the conduction bands were calculated for the optimized {111} microfaceting row model, as shown in Figure 4b and c. Large surface states, localized at α-Ti, are protruded to vacuum. The center bright spot and the side broad spots (Figure 4a) correspond to the 4-fold coordinated α- and the 5-fold coordinated β-Ti, respectively. Observed STM images are in good agreement with the calculational results.

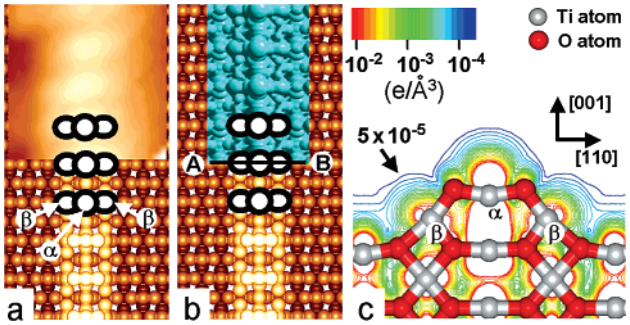

Figure 4. (a) An STM image of TiO_2 (001) isolated row structure (8.6 × 8.5 nm^2, 0.03 nA, 2.5 V). (b) Calculated equi-density surface with a gray surface represents the density level of 1×10^{-4} e/Å^3, and (c) calculated density contour (cut plane is along A−B) of the local wave functions at the bottom of the conduction bands. The equi-electron density surfaces are artificially illuminated from the upper right for the sake of understanding.

We and other groups observed many kinds of surface structures on TiO_2 (001) depending on the sample preparation methods. Our calculational results suggest that the surface energy of the reconstructed structure is more stable compared with the unreconstructed (1 × 1) structure. On the other hand, it is considered that surface energies between different kinds of {111} microfaceting structures are not so different. The surface structures may depend on the initial sample conditions, such as the surface roughness, the existence of the oxygen vacancy defects, the very tiny differences of the stoichiometry in the bulk crystal, and so on, which come from the sample preparations.

As was denoted before, rutile TiO_2 has two stable microfacet faces, i.e., {111} and {110}. We propose {111} microfaceting models to explain the surface reconstructions on (001) and other faces. On the other hand, the surfaces, which are perpendicular to the (001) surface, can be terminated by the microfacet of {110}. For example, it is generally accepted that the {110} microfaceting models explain the reconstructions on the (100) surface.[4] To reduce surface energy, each surface is considered to reconstruct to form a microfaceted surface that exposes stable {111} or (and) {110}. The diversity of the surface structures originates in the diversity of the combination of microfacets.

Finally, it is noted that the microfaceting reconstructions do not explain all the structures on rutile TiO_2 surfaces. In fact, it is now generally accepted that the TiO_2 (110)−(1 × 2) structure is due to the nonstoichiometric Ti_2O_3 added row.[4] In the field of metal oxide surface science, it has been widely believed that the complicated structures are generally related to nonstoichiometric suboxide structures. We proposed a different concept of the reconstruction, which makes the numerous numbers of complicated structures clear.

V. Summary and Conclusion

In this paper, we have used STM, XPS, and density functional calculations to elucidate the nature of the surface reconstructions on rutile TiO_2 surfaces. We propose microfaceting structural models that expose the stable planes. This model explains experimental results well and gives an additional reason the rutile TiO_2 exhibits various surface structures.

JA0578808